NANO LETTERS

Letter

pubs.acs.org/NanoLett

Highly Active and Durable Core–Corona Structured Bifunctional Catalyst for Rechargeable Metal–Air Battery Application

Zhu Chen, Aiping Yu, Drew Higgins, Hui Li, Haijiang Wang, and Zhongwei Chen*

Department of Chemical Engineering, Waterloo Institute for Nanotechnology, and Waterloo Institute for Sustainable Energy, University of Waterloo, Waterloo, ON, Canada N2L 3G1

Supporting Information

ABSTRACT: A new class of core–corona structured bifunctional catalyst (CCBC) consisting of lanthanum nickelate centers supporting nitrogen-doped carbon nanotubes (NCNT) has been developed for rechargeable metal–air battery application. The nanostructured design of the catalyst allows the core and corona to catalyze the oxygen evolution reaction (OER) and oxygen reduction reaction (ORR), respectively. These materials displayed exemplary OER and ORR activity through half-cell testing, comparable to state of the art commercial lanthanum nickelate ($LaNiO_3$) and carbon-supported platinum (Pt/C), with added bifunctional capabilities allowing metal–air battery rechargeability. $LaNiO_3$ and Pt/C are currently the most accepted benchmark electrocatalyst materials for the OER and ORR, respectively; thus with comparable activity toward both of these reactions, CCBC are presented as a novel, inexpensive catalyst component for the cathode of rechargeable metal–air batteries. Moreover, after full-range degradation testing (FDT) CCBC retained excellent activity, retaining 3 and 13 times greater ORR and OER current upon comparison to state of the art Pt/C. Zinc–air battery performances of CCBC is in good agreement with the half-cell experiments with this bifunctional electrocatalyst displaying high activity and stability during battery discharge, charge, and cycling processes. Owing to its outstanding performance toward both the OER and ORR, comparable with the highest performing commercial catalysts to date for each of the respective reaction, coupled with high stability and rechargeability, CCBC is presented as a novel class of bifunctional catalyst material that is very applicable to future generation rechargeable metal–air batteries.

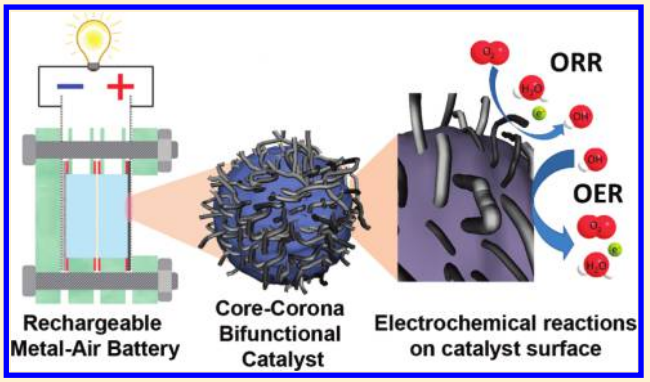

KEYWORDS: *Metal–air batteries, core–corona, bifunctional catalyst, nitrogen-doped carbon nanotubes, metal oxides*

Growing global interest in electric vehicles (EV) requires smaller and lighter rechargeable batteries to meet the energy and environmental challenges of the world. Rechargeable Li ion batteries are traditionally considered the most promising contenders for EV applications due to their high cycle capability and energy efficiency.[1−5] However, insufficient storage capacity of lithium ion batteries (100–200 W h kg^{-1}) limits its long-term application in EVs.[6−9] Recently, rechargeable metal–air batteries such as zinc–air batteries and lithium–air batteries have attracted much attention as a possible alternative owing to their extremely high energy density (470 and 1700 W h kg^{-1}, respectively), low cost, and environmentally friendly operation.[7,10] Metal–air batteries are compact, lightweight, and cost-effective because they employ a lighter cathode operating on environmentally abundant oxygen from the air during discharge, replacing expensive chemical constituents used in current rechargeable lithium ion batteries. Nonetheless, the rechargeable metal–air batteries are still in their early stages of development due to existing technical hurdles including poor durability, limited performance, and high cost.

Inadequate durability and performance of metal–air batteries are most commonly attributed to limitations stemming from the existing catalysts utilized for the oxygen reduction reaction (ORR) and oxygen evolution reactions (OER), limiting the practical use of these metal–air batteries.[11−14] At the current state of technology, precious metals and alloys, such as Pt, Pt–Au, and Pt–Pd, have been studied and developed as the best performance bifunctional catalysts for metal–air batteries.[15−23] However, insufficient performance coupled with the limited availability and high cost of these precious metal-based bifunctional catalysts limit their long-term practical application in the metal–air batteries. Therefore, there are no commercially available bifunctional catalyst materials with practical battery performance, and thus it is extremely important to develop inexpensive, corrosion-resistant, and highly active bifunctional catalysts for both the ORR and OER in metal–air batteries.

Herein, we propose a new class of core–corona bifunctional catalyst (CCBC), where the design is based upon a highly ORR

Received: December 15, 2011
Revised: February 19, 2012
Published: February 28, 2012

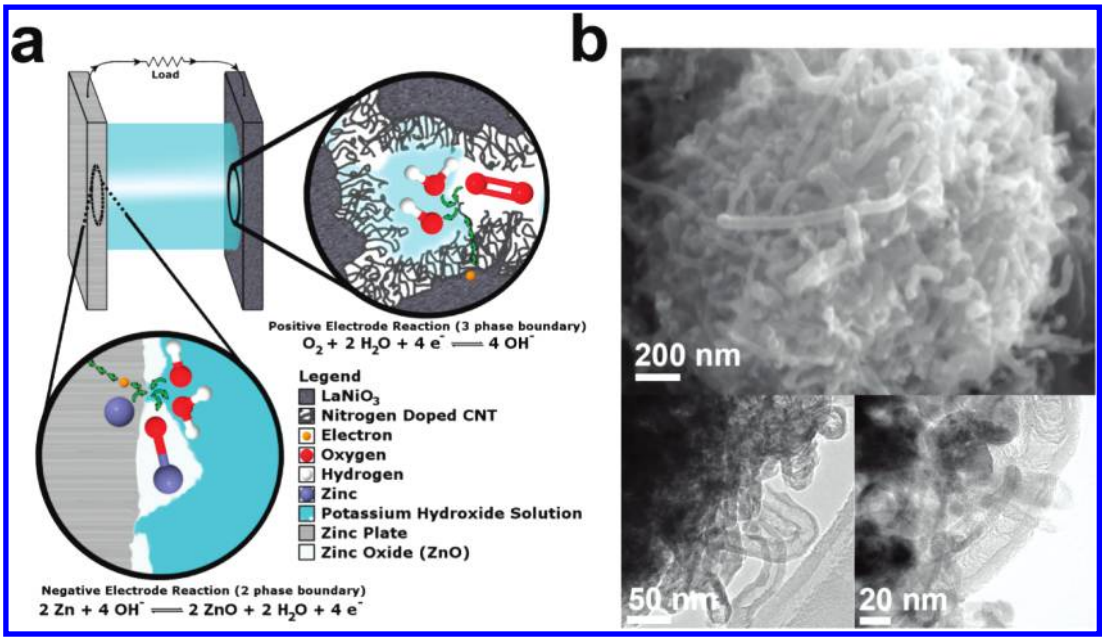

Figure 1. Design and application of the CCBC toward metal−air battery. (a) Schematic of zinc−air battery and the reactions taking places on the electrodes. The CCBC catalyst is applied onto the positive electrode which catalyzes the ORR and OER reactions. (b) Scanning electron micrograph and transmission electron micrograph of the CCBC illustrating the NCNT on the surface of the core particle.

active nitrogen-doped carbon nanotube (NCNTs) corona component and a highly OER-active lanthanum nickelate ($LaNiO_3$) derived core component (Figure 1a). $LaNiO_3$ was selected as the core structure, as it is deemed among the top performance materials for OER catalysis readily available to date. Furthermore, not only does the $LaNiO_3$ participate in the formation of a well-defined OER-active core,[24] it also acts as the support material for the synthesis of NCNTs via a simplistic chemical vapor deposition (CVD) method. Previously, perovksite oxides such as $La_{0.6}Ca_{0.4}CoO_3$ and $La_{0.6}Sr_{0.4}CoO_3$ have been used as substrates and catalysts for the synthesis of undoped carbon nanotube (CNT). The resultant composites were tested for electrochemical applications. However, the CNT/perovskite composite showed no decrease in ORR overpotential, and the study toward catalyst stability was lacking. In the proposed CCBC structure, the NCNTs serve as the highly active ORR electrocatalyst component,[14,25−28] while also providing synergistic OER activity. Furthermore, NCNTs are highly graphitic, resulting in robust operational durability, and possess exemplary electronic conductivity, resulting in electron transfer pathways between the CCBC particles.

Scanning electron microscopy (SEM) and transmission electron microscopy (TEM) of the uniquely designed nanostructures confirmed the formation of carbon tubules (Figure 1b) observed on the surface of CCBC to be NCNTs with a bamboo-like structure (Figure 1b). High-resolution X-ray photoelectron spectroscopy (XPS) signals were obtained for the N 1s spectra which was deconvoluted into four contributions: the pyridinic, pyrrolic, quaternary, and pyrrolidone nitrogen groups (Figure S6 and Table S2). These observed surface nitrogen groups are consistent with previously reported data for nitrogen-doped carbon materials.[25,27,29−39] Based on XPS analysis, the pyridinic and pyrrolic nitrogen groups were found to be the most dominant surface nitrogen configurations. These surface nitrogen groups have been previously directly correlated to ORR activity and are desirable in high concentrations.[26,27] To provide details on the growth of the NCNT corona structures, the synthesis of CCBC was interrupted at various stages of growth based on the amount of NCNT precursor material injected into the CVD system. When large volumes of precursor solution was injected into the system, long and dense forestation of NCNT on the surface of CCBC is evident from the comparison of SEM and TEM (see Figures S4 and S5). Utilizing smaller precursor volumes resulted in the formation of relatively shorted, sparse NCNT coverage (Figures S4 and S5). Optimization of the CCBC catalyst with respect to the amount of precursor solution utilized reveals that the most active catalyst, CCBC-2, can be synthesized using 2 mL of precursor solution (Figure S13). Thermogravimetric analysis of CCBC-2 indicates that carbon and metal oxides constitutes 64.2 and 35.8 wt % of the CCBC-2 catalyst, respectively (Figure S7).

Half-cell testing was employed to evaluate the ORR and OER activities of the CCBC-2. Comparison of ORR and OER activity was made with commercial Pt/C and $LaNiO_3$, respectively, as these materials are deemed the highest performing state of the art catalyst materials toward the respective reactions.[30,40,41] Excellent ORR activity was demonstrated by the CCBC-2, where the half-wave potential and ORR current density are very similar to the commercial Pt/C. In comparison to the $LaNiO_3$, CCBC-2 illustrates 5.8 times higher ORR current density at −0.5 V and a 200 mV improvement in half-wave potential. The much higher ORR performance of CCBC-2 over $LaNiO_3$ suggests that the NCNT corona is responsible for the excellent ORR activity of CCBC-2. The number of electrons transfer during ORR is calculated for CCBC-2 and $LaNiO_3$ using the Koutecky−Levich equation (Figure S12 and Table S3). The CCBC-2 catalyst demonstrates a four-electron reduction of oxygen, significantly more efficient compared to the two-electron reduction determined for $LaNiO_3$. ORR occurring by a more efficient pathway indicates the irrefutable impact of the NCNT corona on the overall activity of the CCBC-2 catalyst. Apart from high ORR activity, excellent OER activity is considered another vital characteristic

dx.doi.org/10.1021/nl2044327 | *Nano Lett.* 2012, 12, 1946−1952

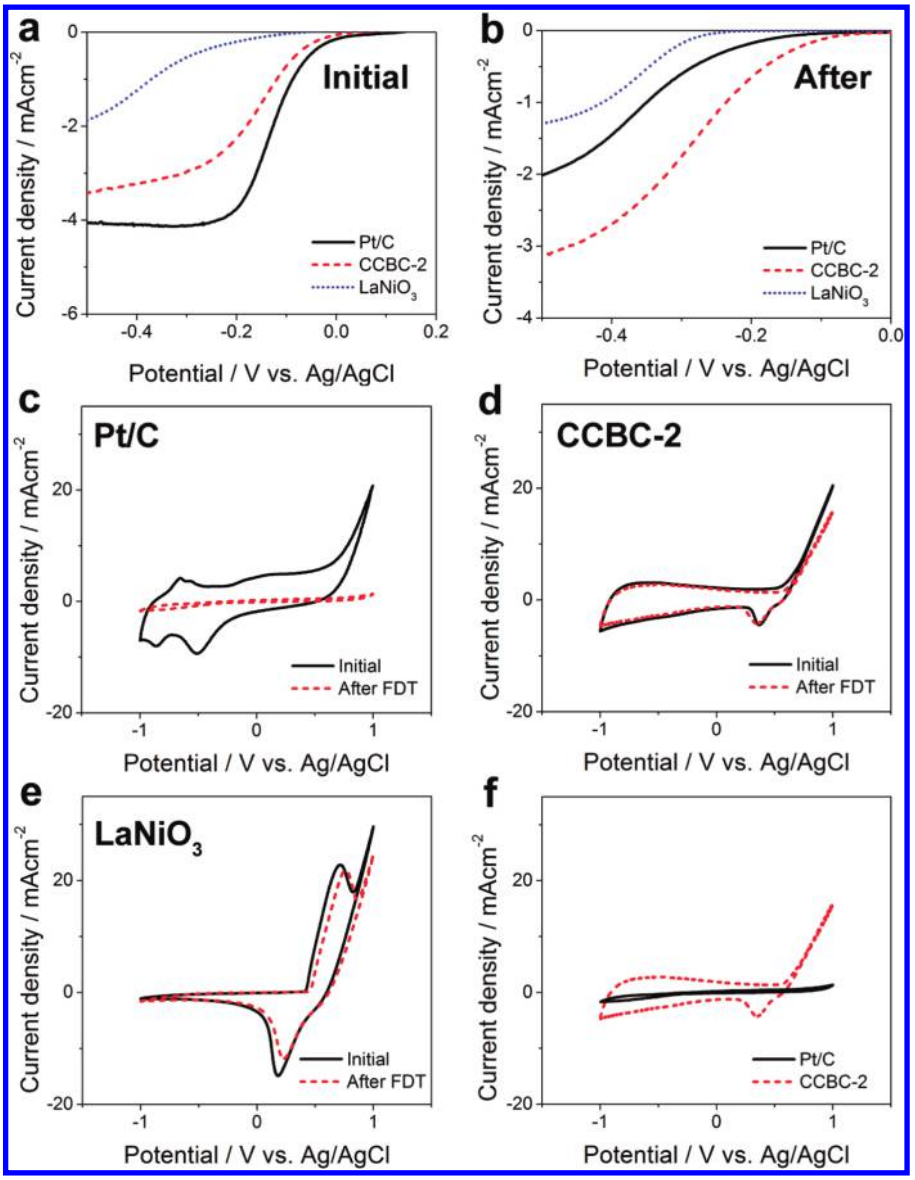

Figure 2. Half-cell performance of Pt/C, CCBC-2, and $LaNiO_3$ measured by a rotating ring disk electrode system. Polarization curves of Pt/C, CCBC-2, and $LaNiO_3$ (a) before FDT and (b) after FDT. Cyclic voltammogram and OER performance of (c) Pt/C, (d) CCBC-2, and (e) $LaNiO_3$. (f) Comparison of the OER activity of Pt/C and the CCBC-2 after FDT.

of bifunctional catalyst materials. Despite a much lower overall composition of the core $LaNiO_3$ material, the initial OER current density of the CCBC-2 is comparable with $LaNiO_3$ at 1 V vs Ag/AgCl (Figure 2d,e), indicating exemplary OER kinetics.

Table 1. Summary of the Half-Cell Test Results from Pt/C, CCBC-2, $LaNiO_3$, and NCNT[a]

	before FDT		after FDT	
	J_{ORR}/ mA cm^{-2}	J_{OER}/ mA cm^{-2}	J_{ORR}/ mA cm^{-2}	J_{OER}/mA cm^{-2}
Pt/C	−4.12	20.7	−0.621	1.22
CCBC-2	−3.00	20.5	−1.77	19.6* and 15.8
$LaNiO_3$	−0.520	29.5	−0.180	24.4
NCNT	−3.67	8.14	−0.110	0.890*

[a] J_{ORR} and J_{OER} represent the ORR and OER current densities, respectively. The J_{ORR} was measured at −0.3 V, and J_{OER} was measured at 1 V. Potentials were measured versus a double junction Ag/AgCl reference electrode. All the ORR and OER performances after the FDT were measured after 500 cycles, unless indicated by an asterisk, in which case the measurements were taken after 100 cycles.

While ORR and OER activity are important parameters for the development of bifunctional catalyst materials, catalyst stability is also critical for practical applications. To investigate this, full-range degradation testing (FDT) was performed using cyclic voltammetry in the range of −1 to 1 V vs Ag/AgCl on catalyst samples (Figure 2c−e). The commercial Pt/C catalyst suffered from significant performance degradation after FDT (Figure 2b,c), whereas CCBC-2 demonstrated excellent stability exhibiting 3 and 13 times higher ORR and OER current density, respectively, following FDT. Under the high potentials incurred during FDT, Pt/C degradation could occur via particle agglomeration, dissolution, surface oxide formation, or detachment from the carbon support due to corrosion. Based on the CV profile of Pt/C, a significant decrease in capacitive current and the disappearance of hydrogen adsorption/desorption peaks suggest dramatic changes to the

dx.doi.org/10.1021/nl2044327 | Nano Lett. 2012, 12, 1946−1952

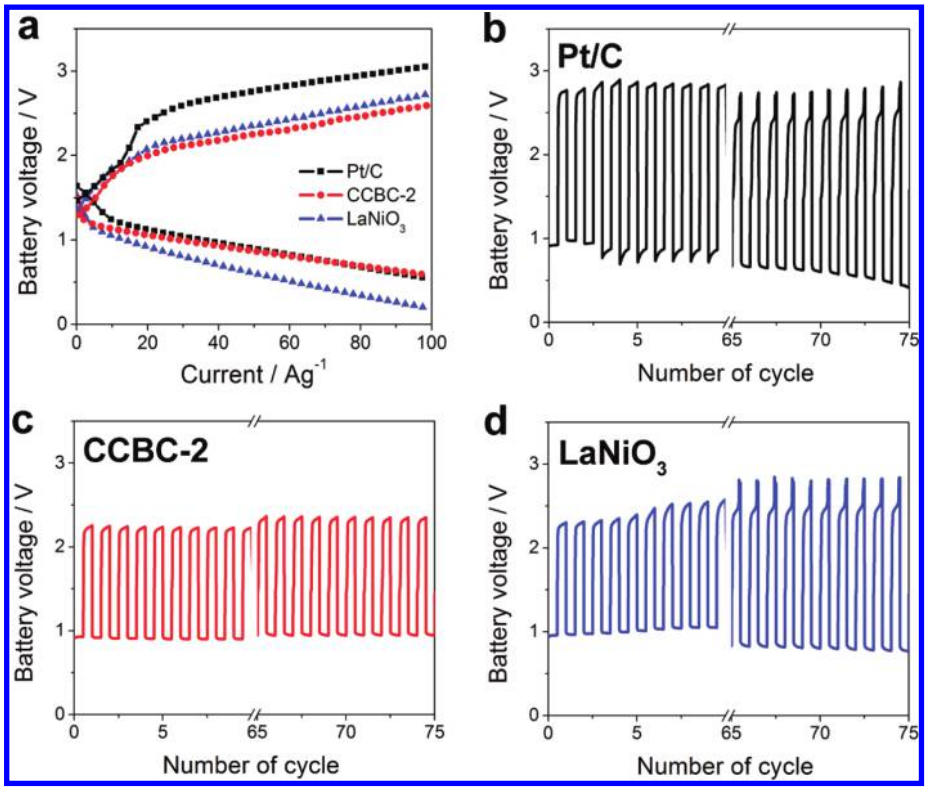

Figure 3. Zinc–air battery performance of the Pt/C, CCBC-2, and $LaNiO_3$. (a) Discharge and charge polarization curves of Pt/C, CCBC-2, and $LaNiO_3$. C–D cycling of (b) Pt/C, (c) CCBC-2, and (d) $LaNiO_3$. One discharge and charge is referred to as one cycle, and the battery was cycled 75 times.

Table 2. Summary of the Battery Test Results from Pt/C, CCBC-2, and $LaNiO_3$[a]

	E_{OCV}/V	$I_{discharge}$/A g^{-1}	I_{charge}/A g^{-1}
Pt/C	1.48	62.0	13.3
CCBC-2	1.45	60.5	20.2
$LaNiO_3$	1.45	29.4	17.2

[a] E_{OCV} denotes open-circuit potential. $I_{discharge}$ and I_{charge} represent the mass specific discharge and charge current densities obtained at 0.8 and 2 V, respectively.

catalyst surface structures, most likely according to the aforementioned degradation mechanisms. In sharp contrast, the CCBC-2 is durable under continuous cycling, which is apparent from the stable CV profile (Figure 2). During battery charging, the bifunctional catalyst materials will be exposed to very high electrode potentials during the OER, which is conducive to surface oxidation and degradation. Thus, retaining ORR activity after experiencing these elevated potentials is a significant challenge facing bifunctional catalyst materials, primarily those composed of carbon. Despite these high potentials encountered during FDT, CCBC-2 retained its high activity. This indicates that the oxidation of the NCNT materials was not prevalent and that the unique core–corona structure potentially improves the overall stability of the catalyst. A synergistic effect could exist between the core material and the NCNT corona of the CCBC-2, where the enhanced stability of the NCNT corona could be influenced by the core material assisting in the prevention of carbon corrosion. This potential interaction is clearly demonstrated by comparing the catalyst performance loss of pure NCNT and CCBC-2 following FDT. The ORR and OER current density of NCNT decreased by 97% and 89%, respectively (Figure S8); meanwhile, the CCBC-2 catalyst only demonstrated a 25% and 10% decrease in the ORR and OER current density, respectively. It can be concluded that the observed synergistic effect and stable catalyst structure arising from the unique core–corona configuration provides the key for the catalyst's exemplary bifunctional activity and stability. To further illustrate the advantage of the proposed catalyst design, half-cell performances of carbon (Ketjenblack) supported $LaNiO_3$ and $LaNiO_3$/NCNT catalyst prepared by simple physical mixing are included in the Supporting Information (Figures S15, S16, and S18). The CCBC-2 catalyst compares favorably to the carbon supported $LaNiO_3$ and $LaNiO_3$/NCNT in terms of bifunctional activity and stability. Combining $LaNiO_3$ and NCNT into one entity—the CCBC—can increase catalyst durability as a result of strong physical connections between the NCNT and core material. In addition, more homogeneous dispersion of NCNT around the core material and throughout the entire catalyst sample as well as decreased electrode inhomogeneity can contribute to the superior performance of the CCBC catalyst.

Building on the promising half-cell performance, metal–air battery adopting a zinc electrode was used to evaluate the catalyst's performance under realistic operating conditions. In this study CCBC-2 was compared to the Pt/C and $LaNiO_3$ for discharge and charge performance, respectively (Figure 3a and Table 2). The CCBC-2 catalyst demonstrated similar discharge and charge current compared to Pt/C and $LaNiO_3$, indicating that its performance is close to the benchmark materials in ORR and OER. Concurrently, CCBC-2 demonstrated 1.5 times in charge current compared to Pt/C and 1 time higher discharge current compared to $LaNiO_3$. These results testify to

dx.doi.org/10.1021/nl2044327 | *Nano Lett.* 2012, 12, 1946–1952

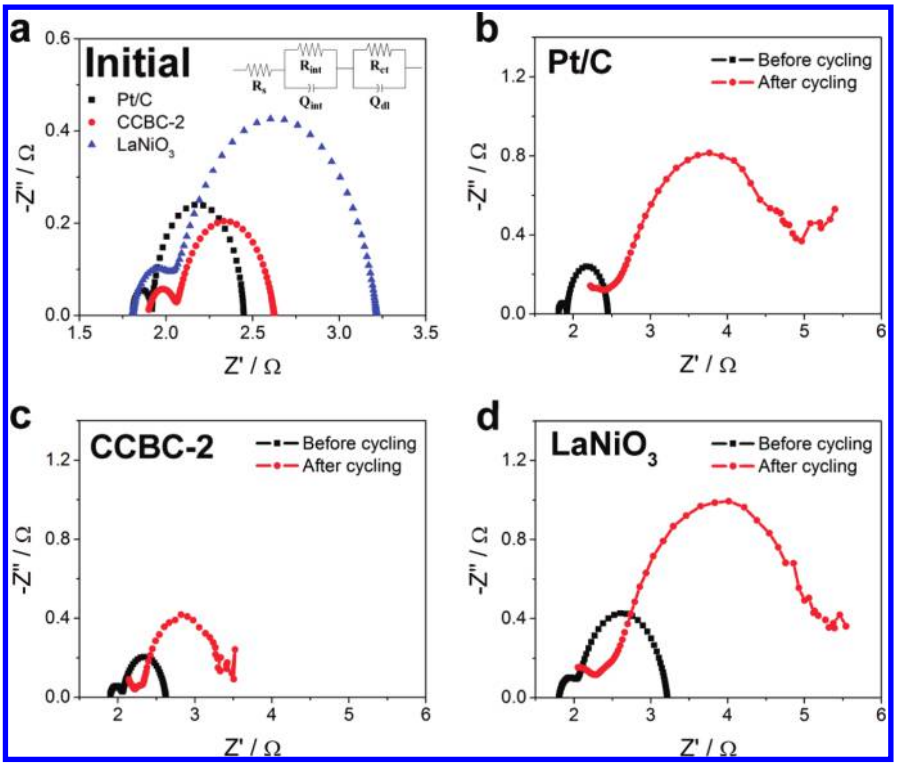

Figure 4. Electrochemical impedance spectroscopy of the zinc–air battery before and after cycling. (a) Initial Nyquist plot of Pt/C, CCBC-2, and $LaNiO_3$. The equivalent circuit is shown. Change in the Nyquist plot as a result of C–D cycling: (b) Pt/C, (c) CCBC-2, and (d) $LaNiO_3$.

Table 3. Summary of the Equivalent Circuit Elements Resulting from Fitting the Impedance Data of Pt/C, CCBC-2, and $LaNiO_3$[a]

	Pt/C	CCBC-2	$LaNiO_3$
R_s (Ω)	1.81	1.89	1.81
R_{int} (Ω)	0.110	0.168	0.242
R_{ct} (Ω)	0.531	0.562	1.17
Q_{int} ($S{\cdot}s^n$)	2.11×10^{-4}	3.58×10^{-2}	1.36×10^{-3}
Q_{dl} ($S{\cdot}s^n$)	8.57×10^{-2}	5.45×10^{-4}	2.50×10^{-2}

[a]The electrochemical impedance spectroscopy was performed at 0.8 V with 20 mV ac potential from 100 kHz to 0.1 Hz.

the excellent bifunctional activity of CCBC-2, which is a powerful advantage with regards to catalyst stability during battery cycling. The rechargeability of the CCBC-2 catalyst was evaluated by charge–discharge (C–D) cycling experiments (Figure 3b–d and Table S4). For an active bifunctional catalyst, low charge potential (E_{charge}), high discharge potential ($E_{discharge}$), and minimal fluctuation of these are required for good rechargeability. After C–D cycling, the $E_{discharge}$ of CCBC-2 remained unchanged after 75 cycles. In contrast, Pt/C and $LaNiO_3$ suffered a 20% and 56% decrease in $E_{discharge}$, respectively. With respect to battery charge, CCBC-2 shows ~22% lower E_{charge} compared to Pt/C and $LaNiO_3$ after C–D cycling. C–D cycling results of carbon supported $LaNiO_3$ and $LaNiO_3$/NCNT are included in the Supporting Information (Figures S16 and S18). Conducting C–D cycling of these two materials results in significant degradation to the battery performances, which is in sharp contrast to the high stability observed for the CCBC-2 coated air electrode. The outstanding cycling performance further emphasizes the great potential of the CCBC catalyst for rechargeable metal–air battery application.

In order to understand the high stability of the CCBC catalyst, electrochemical impedance spectroscopy was performed. The impedance data are fitted using an equivalent circuit (Figure S14, Supporting Information), and the values of fitted parameters are reported in Table 3. Nyquist plots (Figure 4) reveal that the charge transfer resistance (R_{ct}) value CCBC-2 is similar to Pt/C and 52% lower compared to $LaNiO_3$. Thus, the smaller R_{ct} values of CCBC-2 compared with $LaNiO_3$ is a strong indication of the improvement in ORR kinetics. Similar impedance study was carried out during battery charging at 2 V. Fitting of the impedance data by an equivalent circuit is presented in the Supporting Information (Figure S19). Based on the analysis, the CCBC-2 catalyst illustrates lowest R_{ct} followed by $LaNiO_3$. Meanwhile, the Pt/C catalyst displays nearly 10 times greater R_{ct} value. The trend observed in the initial values of R_{ct} during battery operation (charge or discharge) accurately reflects the activity of each catalyst presented in Figure 3a. After cycling, the value of R_{ct} during battery discharge increased by approximately 2 and 4 times for the Pt/C and $LaNiO_3$, respectively. To the contrary, CCBC-2 showed markedly less increase in R_{ct}, which is in agreement with the C–D cycling performance shown in Figure 3. The variation in the value of R_{ct} could be a partial reason for the high stability observed for CCBC-2.

To the best of our knowledge, this report is the first to illustrate the successful synthesis of a CCBC from NCNT and $LaNiO_3$ as well as its application in a rechargeable metal–air battery. Based on physiochemical characterizations, the formation of a core–corona structure was confirmed. The CCBC-2 displayed excellent bifunctional activity and stability compared with Pt/C and $LaNiO_3$ based on the half-cell tests. In addition, the charge and discharge performance of the CCBC-2 evaluated using a zinc–air battery show great potential application. Further characterization of the core–corona

dx.doi.org/10.1021/nl2044327 | Nano Lett. 2012, 12, 1946–1952

structure and additional electrochemical studies are underway to understand the physical origin of the catalyst's high activity and stability. Based on the promising results obtained in this study, the proposed core−corona structure concept has been proven to be outstanding for ORR and OER catalysis and more specifically for applications in rechargeable zinc−air batteries. The remarkable potential displayed by this type of CCBC warrants further study and could facilitate the large-scale implementation of rechargeable metal−air batteries.

■ ASSOCIATED CONTENT

Supporting Information

Additional figures, tables, and discussion depicting experimental results. This material is available free of charge via the Internet at http://pubs.acs.org.

■ AUTHOR INFORMATION

Corresponding Author

*E-mail zhwchen@uwaterloo.ca; Tel 1-519-888-4567 ext 38664; Fax 1-519-746-4979.

Notes

The authors declare no competing financial interest.

■ ACKNOWLEDGMENTS

This research was supported by the Natural Sciences and Engineering Research Council of Canada (NSERC), the University of Waterloo, and the Waterloo Institute for Nanotechnology. The authors thank Dr. Shaomin Zhu, Mr. Drew Higgins, Mr. Jason Wu, and Mr. Ryan S. Hsu at the University of Waterloo for their help in editing the manuscript.

■ REFERENCES

(1) Chan, C. K.; Peng, H. L.; Twesten, R. D.; Jarausch, K.; Zhang, X. F.; Cui, Y. Fast, completely reversible Li insertion in vanadium pentoxide nanoribbons. *Nano Lett.* **2007**, *7*, 490−495.

(2) Cui, L. F.; Yang, Y.; Hsu, C. M.; Cui, Y. Carbon-Silicon Core-Shell Nanowires as High Capacity Electrode for Lithium Ion Batteries. *Nano Lett.* **2009**, *9*, 3370−3374.

(3) Lee, H. W.; Muralidharan, P.; Ruffo, R.; Mari, C. M.; Cui, Y.; Kim, D. K. Ultrathin Spinel LiMn(2)O(4) Nanowires as High Power Cathode Materials for Li-Ion Batteries. *Nano Lett.* **2010**, *10*, 3852−3856.

(4) Park, M. H.; Kim, M. G.; Joo, J.; Kim, K.; Kim, J.; Ahn, S.; Cui, Y.; Cho, J. Silicon Nanotube Battery Anodes. *Nano Lett.* **2009**, *9*, 3844−3847.

(5) Zheng, G. Y.; Yang, Y.; Cha, J. J.; Hong, S. S.; Cui, Y. Hollow Carbon Nanofiber-Encapsulated Sulfur Cathodes for High Specific Capacity Rechargeable Lithium Batteries. *Nano Lett.* **2011**, *11*, 4462−4467.

(6) Lukic, S. M.; Cao, J.; Bansal, R. C.; Rodriguez, F.; Emadi, A. Energy storage systems for automotive applications. *IEEE Trans. Ind. Electron.* **2008**, *55*, 2258−2267.

(7) Girishkumar, G.; McCloskey, B.; Luntz, A. C.; Swanson, S.; Wilcke, W. Lithium - Air Battery: Promise and Challenges. *J. Phys. Chem. Lett.* **2010**, *1*, 2193−2203.

(8) Wagner, F. T.; Lakshmanan, B.; Mathias, M. F. Electrochemistry and the Future of the Automobile. *J. Phys. Chem. Lett.* **2010**, *1*, 2204−2219.

(9) Scrosati, B.; Garche, J. Lithium batteries: Status, prospects and future. *J. Power Sources* **2010**, *195*, 2419−2430.

(10) Lee, J. S.; Tai Kim, S.; Cao, R.; Choi, N. S.; Liu, M.; Lee, K. T.; Cho, J. Metal-Air Batteries with High Energy Density: Li-Air versus Zn-Air. *Adv. Energy Mater.* **2010**, *1*, 34−50.

(11) Lee, J. S.; S., P. G.; Lee, H. I.; Kim, S. T.; Cao, R. G.; Liu, M. L.; Cho, J. Ketjenblack Carbon Supported Amorphous Manganese Oxides Nanowires as Highly Efficient Electrocatalyst for Oxygen Reduction Reaction in Alkaline Solutions. *Nano Lett.* **2011**, *11*, 5362−5366.

(12) Neburchilov, V.; Wang, H.; Martin, J. J.; Qu, W. A review on air cathodes for zinc-air fuel cells. *J. Power Sources* **2010**, *195*, 1271−1291.

(13) Lu, Y. C.; Kwabi, D. G.; Yao, K. P. C; Harding, J. R.; Zhou, J. G.; Zuin, L.; Shao-Horn, Y. The discharge rate capability of rechargeable Li-O(2) batteries. *Energy Environ. Sci.* **2011**, *4*, 2999−3007.

(14) Chen, Z. W.; Higgins, D.; Yu, A. P.; Zhang, L.; Zhang, J. J. A review on non-precious metal electrocatalysts for PEM fuel cells. *Energy Environ. Sci.* **2011**, *4*, 3167−3192.

(15) Lim, B. W.; Lu, X. M.; Jiang, M. J.; Camargo, P. H. C.; Cho, E. C.; Lee, E. P.; Xia, Y. N. Facile Synthesis of Highly Faceted Multioctahedral Pt Nanocrystals through Controlled Overgrowth. *Nano Lett.* **2008**, *8*, 4043−4047.

(16) Lim, B.; Jiang, M. J.; Camargo, P. H. C.; Cho, E. C.; Tao, J.; Lu, X. M.; Zhu, Y. M.; Xia, Y. N. Pd-Pt Bimetallic Nanodendrites with High Activity for Oxygen Reduction. *Science* **2009**, *324*, 1302−1305.

(17) Chen, J. Y.; Lim, B.; Lee, E. P.; Xia, Y. N. Shape-controlled synthesis of platinum nanocrystals for catalytic and electrocatalytic applications. *Nano Today* **2009**, *4*, 81−95.

(18) Lim, B.; Jiang, M. J.; Yu, T.; Camargo, P. H. C.; Xia, Y. N. Nucleation and growth mechanisms for Pd-Pt bimetallic nanodendrites and their electrocatalytic properties. *Nano Res.* **2010**, *3* (2), 69−80.

(19) Shao, M. H.; Yu, T.; Odell, J. H.; Jin, M. S.; Xia, Y. N. Structural dependence of oxygen reduction reaction on palladium nanocrystals. *Chem. Commun.* **2011**, *47*, 6566−6568.

(20) Yu, T.; Kim, D. Y.; Zhang, H.; Xia, Y. N. Platinum Concave Nanocubes with High-Index Facets and Their Enhanced Activity for Oxygen Reduction Reaction. *Angew. Chem., Int. Ed.* **2011**, *50*, 2773−2777.

(21) Lim, B.; Yu, T. Y.; Xia, Y. N. Shaping a Bright Future for Platinum-Based Alloy Electrocatalysts. *Angew. Chem., Int. Ed.* **2010**, *49*, 9819−9820.

(22) Lee, H.; Habas, S. E.; Kweskin, S.; Butcher, D.; Somorjai, G. A.; Yang, P. Morphological control of catalytically active platinum nanocrystals. *Angew. Chem., Int. Ed.* **2006**, *118*, 7988−7992.

(23) Chen, Z.; Waje, M.; Li, W.; Yan, Y. Supportless Pt and PtPd Nanotubes as Electrocatalysts for Oxygen Reduction Reactions. *Angew. Chem., Int. Ed.* **2007**, *46*, 4060−4063.

(24) Suntivich, J.; May, K. J.; Gasteiger, H. A.; Goodenough, J. B.; Shao-Horn, Y. A Perovskite Oxide Optimized for Oxygen Evolution Catalysis from Molecular Orbital Principles. *Science* **2011**, *334*, 1383−1385.

(25) Chen, Z.; Choi, J. Y.; Wang, H. J.; Li, H.; Chen, Z. W. Highly durable and active non-precious air cathode catalyst for zinc air battery. *J. Power Sources* **2011**, *196*, 3673−3677.

(26) Chen, Z.; Higgins, D.; Chen, Z. W. Nitrogen doped carbon nanotubes and their impact on the oxygen reduction reaction in fuel cells. *Carbon* **2010**, *48*, 3057−3065.

(27) Chen, Z.; Higgins, D.; Tao, H. S.; Hsu, R. S.; Chen, Z. W. Highly Active Nitrogen-Doped Carbon Nanotubes for Oxygen Reduction Reaction in Fuel Cell Applications. *J. Phys. Chem. C* **2009**, *113*, 21008−21013.

(28) Higgins, D.; Chen, Z.; Chen, Z. W. Nitrogen doped carbon nanotubes synthesized from aliphatic diamines for oxygen reduction reaction. *Electrochim. Acta* **2011**, *56*, 1570−1575.

(29) Choi, J. Y.; Hsu, R. S.; Chen, Z. Highly Active Porous Carbon-Supported Nonprecious Metal-N Electrocatalyst for Oxygen Reduction Reaction in PEM Fuel Cells. *J. Phys. Chem. C* **2010**, *114*, 8048−8053.

(30) Lefevre, M.; Proietti, E.; Jaouen, F.; Dodelet, J. P. Iron-based catalysts with improved oxygen reduction activity in polymer electrolyte fuel cells. *Science* **2009**, *324*, 71−74.

(31) Zhu, S. M.; Chen, Z.; Li, B.; Higgins, D.; Wang, H. J.; Li, H.; Chen, Z. W. Nitrogen-doped carbon nanotubes as air cathode catalysts in zinc-air battery. *Electrochim. Acta* **2011**, *56*, 5080−5084.

(32) Gong, K. P.; Du, F.; Xia, Z. H.; Durstock, M.; Dai, L. M. Nitrogen-Doped Carbon Nanotube Arrays with High Electrocatalytic Activity for Oxygen Reduction. *Science* **2009**, *323*, 760−764.
(33) Qu, L. T.; Liu, Y.; Baek, J. B.; Dai, L. M. Nitrogen-Doped Graphene as Efficient Metal-Free Electrocatalyst for Oxygen Reduction in Fuel Cells. *ACS Nano* **2010**, *4*, 1321−1326.
(34) Tang, Y. F.; Allen, B. L.; Kauffman, D. R.; Star, A. Electrocatalytic Activity of Nitrogen-Doped Carbon Nanotube Cups. *J. Am. Chem. Soc.* **2009**, *131*, 13200−13201.
(35) Baker, R.; Wilkinson, D. P.; Zhang, J. Electrocatalytic activity and stability of substituted iron phthalocyanines towards oxygen reduction evaluated at different temperatures. *Electrochim. Acta* **2008**, *53*, 6906−6919.
(36) Bezerra, C. W. B.; Zhang, L.; Lee, K.; Liu, H.; Zhang, J.; Shi, Z.; Marques, A. L. B.; Marques, E. P.; Wu, S. Novel carbon-supported Fe-N electrocatalysts synthesized through heat treatment of iron tripyridyl triazine complexes for the PEM fuel cell oxygen reduction reaction. *Electrochim. Acta* **2008**, *53*, 7703−7710.
(37) Bezerra, C. W. B.; Zhang, L.; Liu, H.; Lee, K.; Marques, A. L. B.; Marques, E. P.; Wang, H.; Zhang, J. A review of heat-treatment effects on activity and stability of PEM fuel cell catalysts for oxygen reduction reaction. *J. Power Sources* **2007**, *173*, 891−908.
(38) Lee, K.; Zhang, L.; Lui, H.; Hui, R.; Shi, Z.; Zhang, J. Oxygen reduction reaction (ORR) catalyzed by carbon-supported cobalt polypyrrole (Co-PPy/C) electrocatalysts. *Electrochim. Acta* **2009**, *54*, 4704−4711.
(39) Liu, H.; Song, C.; Tang, Y.; Zhang, J. High-surface-area CoTMPP/C synthesized by ultrasonic spray pyrolysis for PEM fuel cell electrocatalysts. *Electrochim. Acta* **2007**, *52*, 4532−4538.
(40) Gorlin, Y.; Jaramillo, T. F. A Bifunctional Nonprecious Metal Catalyst for Oxygen Reduction and Water Oxidation. *J. Am. Chem. Soc.* **2010**, *132*, 13612−13614.
(41) Jaouen, F.; Dodelet, J. P. O_2 reduction mechanism on non-noble metal catalysts for PEM fuel cells. Part I: Experimental rates of O_2 electroreduction, H_2O_2 electroreduction, and H2O2 disproportionation. *J. Phys. Chem. C* **2009**, *113*, 15422−15432.